LANGMUIR

Article

pubs.acs.org/Langmuir

Colloidal Properties of Nanoerythrosomes Derived from Bovine Red Blood Cells

Yuan-Chia Kuo,[†,‡] Hsuan-Chen Wu,[†,§] Dao Hoang,[∥] William E. Bentley,[†] Warren D. D'Souza,*[,†,‡] and Srinivasa R. Raghavan*[,†,∥]

[†]Fischell Department of Bioengineering, University of Maryland, College Park, Maryland 20742, United States

[‡]Department of Radiation Oncology, University of Maryland School of Medicine, Baltimore, Maryland 21201, United States

[§]Department of Biochemical Science and Technology, National Taiwan University, Taipei 10617, Taiwan

[∥]Department of Chemical and Biomolecular Engineering, University of Maryland, College Park, Maryland 20742, United States

ABSTRACT: Liposomes are nanoscale containers that are typically synthesized from lipids using a high-shear process such as extrusion or sonication. While liposomes are extensively used in drug delivery, they do suffer from certain problems including limited colloidal stability and short circulation times in the body. As an alternative to liposomes, we explore a class of container structures derived from erythrocytes (red blood cells). The procedure involves emptying the inner contents of these cells (specifically hemoglobin) and resuspending the empty structures in buffer, followed by sonication. The resulting structures are termed nanoerythrosomes (NERs), i.e., they are membrane-covered nanoscale containers, much like liposomes. Cryo-transmission electron microscopy (cryo-TEM) and small-angle neutron scattering (SANS) are employed for the first time to study these NERs. The results reveal that the NERs are discrete spheres (~110 nm diameter) with a unilamellar membrane of thickness ~4.5 nm. Remarkably, the biconcave disc-like shape of erythrocytes is also exhibited by the NERs under hypertonic conditions. Moreover, unlike typical liposomes, NERs show excellent colloidal stability in both buffer as well as in serum at room temperature, and are also able to withstand freeze−thaw cycling. We have explored the potential for using NERs as colloidal vehicles for targeted delivery. Much like conventional liposomes, NER membranes can be decorated with fluorescent or other markers, solutes can be encapsulated in the cores of the NERs, and NERs can be targeted to specifically bind to mammalian cells. Our study shows that NERs are a promising and versatile class of nanostructures. NERs that are harvested from a patient's own blood and reconfigured for nanomedicine can potentially offer several benefits including biocompatibility, minimization of immune response, and extended circulation time in the body.

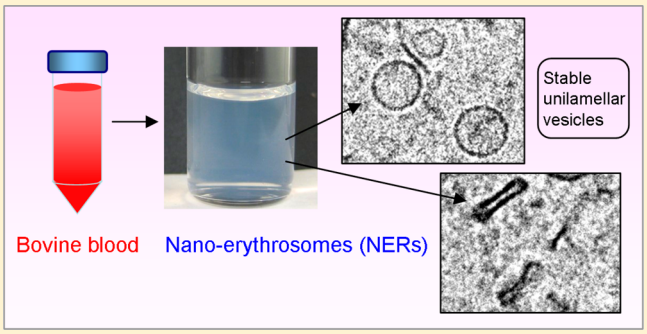

INTRODUCTION

Liposomes are enclosed containers made from biological lipids.[1−8] They were first synthesized by Bangham in 1964,[2] and have been studied extensively since. To prepare liposomes, the starting materials are usually lipids, i.e., two-tailed amphiphiles, such as phosphatidylcholine (PC) derived from egg. Since lipids are insoluble in water, they have to be forced into water to induce the assembly of liposomes.[4,5] Typically, this is done by a high-shear process, such as extrusion of a lipid/water mixture through a porous filter, or by sonication.[4,8] The resulting liposomes typically have nanoscale diameters (~100−200 nm) and a unilamellar bilayer membrane. Liposomes can be made to encapsulate solutes of interest such as drugs or proteins, and they can also be endowed with specific biochemical properties through moieties attached to the membrane.[7,9,10] Thus, liposomes are a versatile class of colloidal vehicles for pharmaceutical and biomedical applications, especially for targeted drug delivery to tumors in the body.[6,7]

A noteworthy aspect about liposomes is that they mimic the structure of a typical biological cell, in that both liposomes and cells have a lipid membrane enclosing internal contents.[3,5] However, liposomes also suffer from some problems, especially that of limited colloidal stability, i.e., they often aggregate or fuse when stored at room temperature.[11,12] The lack of stability arises because liposomes do not represent a thermodynamically stable phase; this is particularly evident from the fact that high shear is needed to form these structures.[5] Colloidal stability can be improved by attaching hydrophilic polymers[12−14] or nanoparticles[15] to the liposomal surface−specifically, chains of polyethylene glycol (PEG). The presence of PEG chains sterically stabilizes the liposomes and thus improves their stability;[12−14] however, optimal stability is obtained only for

Received: August 12, 2015
Revised: December 4, 2015
Published: December 18, 2015

DOI: 10.1021/acs.langmuir.5b03014
Langmuir 2016, 32, 171−179

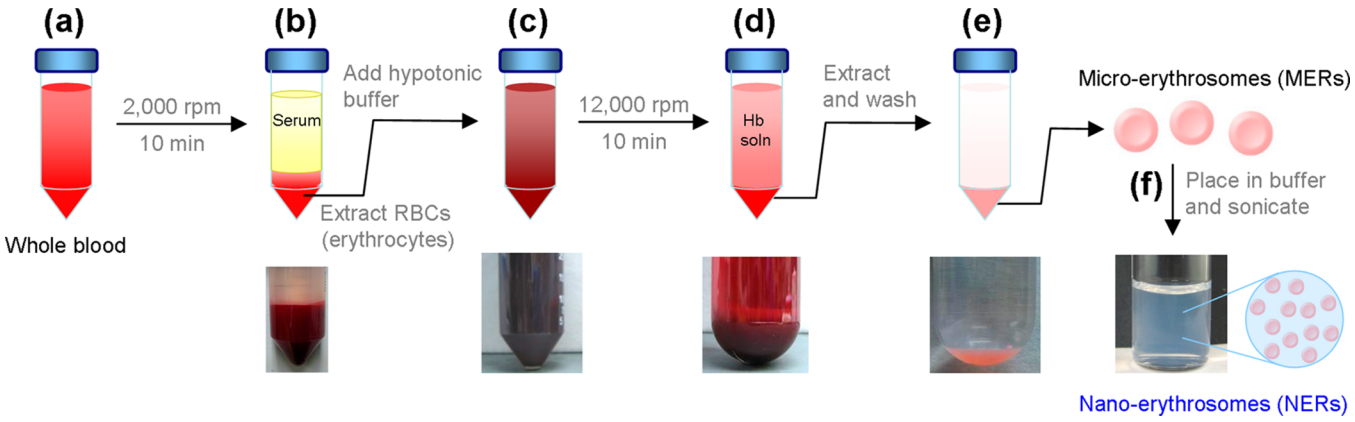

Figure 1. Preparation of nanoerythrosomes (NERs). From bovine whole blood (a), the RBCs are separated (b) and mixed with hypotonic buffer (c) to release the hemoglobin (Hb) in them. Upon centrifugation, the pellet (d) contains the microerythrosomes (MERs), which are then washed and purified (e). A buffer containing the MERs is then sonicated to yield the NERs. Photographs of the sample along the various steps is shown below the schematics. Note that the MER pellet has a light pink-white color. The dispersion of NERs is a homogeneous solution with a bluish tinge due to light scattering from the NERs.

certain lengths and graft densities of PEGs on the liposomes. Thus, researchers who work with liposomes still have to confront stability issues. For example, it is customary to either use liposomal samples right after preparation or after a few days of storage at 4 °C. Liposomal stability is also frequently affected by the media of choice: for example, stability can be poor for liposomes in the presence of blood serum or certain cell-growth media.[16,17] Finally, liposomes can also be destabilized when the sample is subjected to freeze−thaw cycles.[18]

As an alternative to liposomes, one can turn to biological cells and consider the possibility of emptying the contents inside the cells and thereby obtaining the equivalent of liposomes. In this context, erythrocytes, i.e., red blood cells (RBCs), from animal or human sources are particularly easy to empty. These cells have no nucleus or other organelles and also do not contain nucleic acid matter; they are essentially sacs filled with hemoglobin.[19] The idea of using erythrocytes as carriers for a substance other than (or in addition to) hemoglobin dates back to the 1950s.[20−24] Erythrocytes were partially or completely emptied by exposure to hypotonic conditions, and filled with drugs or enzymes.[21,23] These "erythrosomes" (also called "ghosts") were about the same size as the original cells (i.e., around 4 μm in diameter). More recently, in the 1990s, nanoscale analogues of these ghosts were reported by Al-Achi and Boroujerdi[25] and by Lejeune et al.;[26−29] the latter group coined the term "nanoerythrosome" (NER) for these structures. NERs were created by these authors by subjecting the microscale ghosts to a high-shear process, i.e., sonication or extrusion. The resulting structures had nanoscale dimensions (diameters ∼100 to 200 nm) and are thus directly comparable to conventional liposomes.

Although NERs have been known for more than 20 years, they seem to have attracted limited interest from the scientific community. One reason is that their physical, i.e., colloidal properties, have not been systematically studied. For example, we have been unable to find any papers on NERs in traditional journals of colloid science or nanoscience; the few papers that have appeared have all been in pharmaceutical journals.[25−33] In this paper, we report a systematic study of NERs from a colloidal point of view. We use scattering and microscopic techniques to characterize these structures; in particular, the techniques of cryo-transmission electron microscopy (cryo-TEM) and small-angle neutron scattering (SANS) are used for the first time. We have also compared NERs with conventional liposomes prepared from lipids, especially from the viewpoint of colloidal stability and solute encapsulation. Our results confirm that NERs are unique structures with exceptional stability and that they have significant potential for controlled release and targeted drug delivery applications.

RESULTS AND DISCUSSION

Preparation of NERs. The procedure for preparing NERs is shown in Figure 1. We use bovine blood, which has a hematocrit, i.e., volume fraction of erythrocytes, of about 20% (in human blood, the hematocrit is about 40%).[34] In terms of number density, we measured the number density (using a cytometer) of RBCs in the blood used here to be about 3×10^9 cells/mL. RBCs were separated from the white cells, platelets, and serum by centrifugation (Figure 1a), i.e., by exploiting differences in density between the different components. The separated RBCs were then placed in a hypotonic phosphate-buffered saline (PBS) solution.[23,24] This induced the hemoglobin in the cells to leach out due to the osmotic gradient between the cells and the solution (Figure 1c). The process was carried out over a couple of cycles, and at the end, the pellet at the bottom of the tube contained the cells without hemoglobin, which exhibit a characteristic pink or white color (Figure 1e). These are the microerythrosomes (MERs), having diameters around 3 to 4 μm, and they can be resuspended as a stable dispersion either in deionized (DI) water or in a buffer (PBS). The number density measured by the cytometer was 1−1.5×10^9 MERs/mL, i.e., the yield was between 30 to 50%. To reduce their size to the nanoscale, we subjected the dispersion of MERs to high shear using a tip sonicator for 15 min (Figure 1d). This resulted in a stable dispersion of NERs with sizes (see below) around 100 nm. Assuming that the membrane area is conserved during the conversion of MERs to NERs, we estimate the number density of NERs to be about 1.6×10^{12} /mL.

Characterization of NERs. NER sizes were characterized using dynamic light scattering (DLS). DLS yields the hydrodynamic diameter (D_h) of particles assuming that the particles are discrete and noninteracting.[35,36] Figure 2 plots the D_h of NERs in two media: DI water and PBS. In both cases, the

DOI: 10.1021/acs.langmuir.5b03014
Langmuir 2016, 32, 171−179

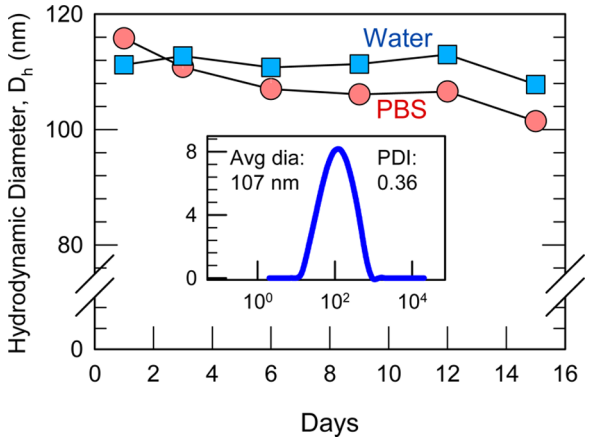

Figure 2. Sizes of NERs over a period of 2 weeks. The sizes correspond to the hydrodynamic diameter D_h from dynamic light scattering (DLS). Data are shown for NERs in PBS (red circles) and in DI water (blue squares). In both cases, the sizes remain nearly unchanged over the period of observation. The inset shows a typical size distribution (intensity% vs diameter) extracted from the DLS data for the NERs. The polydispersity index (PDI) is 0.36.

NERs have a $D_h \sim 105-110$ nm, and this size remains approximately constant over more than 2 weeks of observation. Thus, the NERs show excellent colloidal stability without the need for additional steric stabilizers like PEG. The sizes of NERs are comparable to those of typical liposomes made by extrusion. Polydispersity indices from DLS for the NERs were around 0.3 to 0.4, and these numbers were also similar to those measured for the liposomes. A typical size distribution for the NERs is shown as an inset in Figure 2. We found no significant effect of sonication speed or time on NER size: for example, sonication times between 3 and 15 min gave identical NER sizes (data not shown). In comparison, liposomes typically become smaller if they are sonicated for longer times or at higher shear rates.

Next, the surface charge densities of NERs were measured using zeta potential measurements.[35] The zeta potential was found to range from −30 to −40 mV, indicating a fairly strong negative charge on these structures. The membranes of bovine NERs are expected to consist of phospholipids (∼50%), cholesterol (∼25%) and membrane proteins (∼25%).[37] The net negative charge may arise from anionic phospholipids as well as from anionic membrane proteins. The magnitude of this charge is probably high enough to ensure colloidal stability of the NERs via electrostatic repulsions alone.[35] However, additionally, NERs are also expected to be sterically stabilized by hydrophilic sugar side-chains, attached to either the lipids or the proteins on the external leaflet of the bilayer membrane.[30,35]

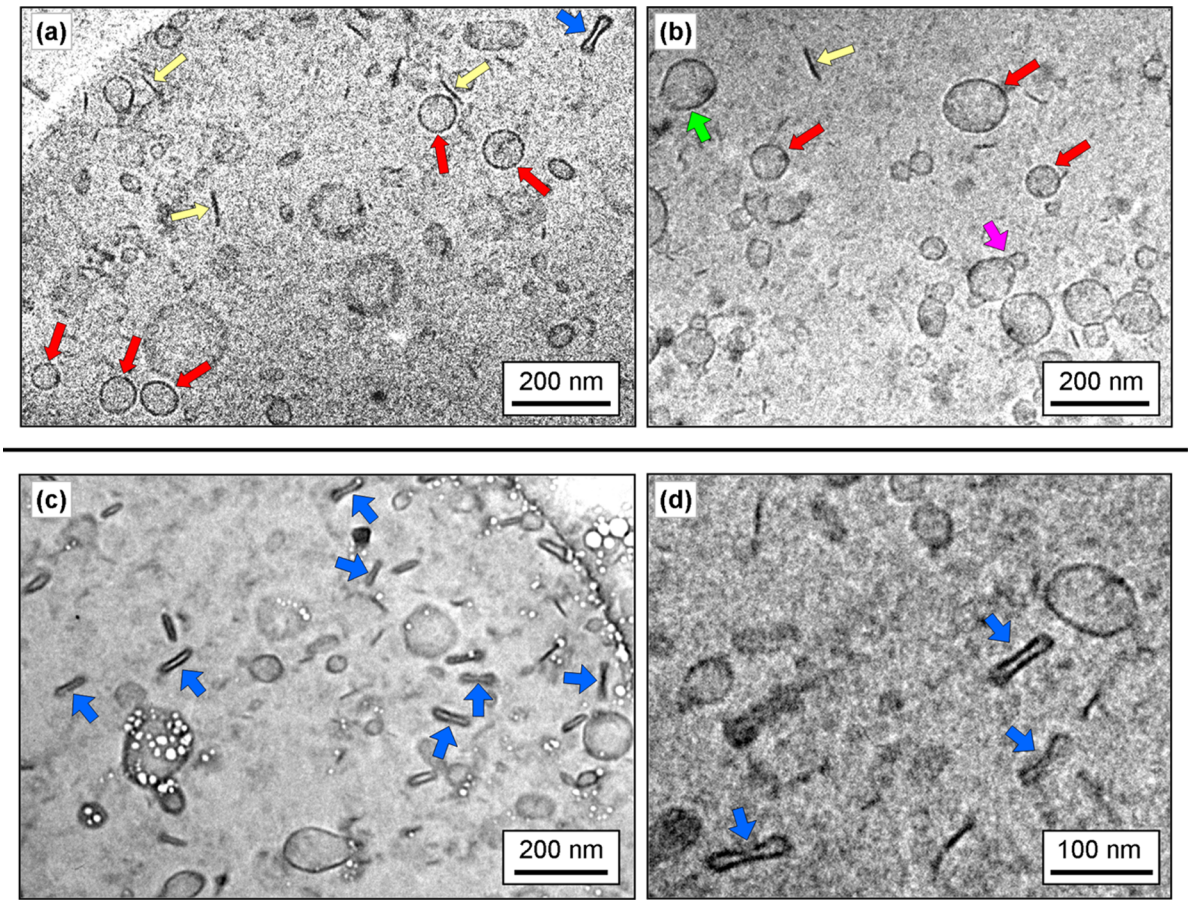

Figure 3. Cryo-TEM micrographs of NERs. Representative images are shown in (a) and (b) for NERs in deionized water and in (c) and (d) for NERs in 2X PBS. Different types of structures are indicated by colored arrows in the images. In (a) and (b) most NERs are intact unilamellar spheres/discs (red arrows). Discs that are lying on their sides appear as straight lines (yellow arrows). Occasionally, a biconcave disc (blue arrow) is seen. Other structures include partially ruptured membranes (green arrow) and fused vesicles (pink arrow). In (c) and (d), most of the NERs are uni- or biconcave discs (blue arrows) due to the hypertonic conditions.

DOI: 10.1021/acs.langmuir.5b03014
Langmuir 2016, 32, 171−179

The morphology of the NERs was then investigated by cryo-TEM.[38−40] In this technique, the structure in an aqueous colloidal sample is preserved by rapid vitrification and then imaged.[38] Cryo-TEM has been extensively used on vesicles and liposomes previously,[39,40] but to our knowledge, not thus far on NERs. Figure 3a,b shows typical cryo-TEM images of NERs suspended in DI water. The most common structures in these image are discrete circles with a thin, dark shell: these correspond to unilamellar vesicles.[39,40] In terms of shape, these could either be spheres or oblate discs viewed from the top. Several instances are also seen of relatively flat discs viewed from their edge, which appear as dark lines on the image.[39,40] Also, the blue arrow indicates one instance of a biconcave disc. Other morphologies are also seen occasionally. For example, in Figure 3b, some unilamellar vesicles appear to be fused at their boundaries into a single structure (pink arrow). Also, the green arrow indicates an incomplete bilayer membrane (disrupted vesicle). For the most part, the structures appear to be intact, and individual structures range in diameter from 90−120 nm, consistent with the size measured by DLS.

We also obtained cryo-TEM images for NERs in 2X PBS buffer (Figure 3c,d). In this environment, which is hypertonic with respect to the NERs, a majority of the NERs adopt a disc like structure. The discs are either uniconcave or biconcave, although this is difficult to determine with certainty. Figure 3d is a close-up of a few NERs that clearly show the biconcave morphology, which is the one usually associated with RBCs. It is known that RBCs are biconcave in an isotonic medium, swell into a more spherical shape in hypotonic media, and shrink and become crenated in hypertonic media.[19] Here also, the NERs are more swollen in water (low osmolarity), but in a hypertonic environment, they mostly exist as concave discs. It is remarkable that the biconcave disc-like shape is still retained in the nanosized NERs! While the exact origin of biconcavity in RBCs is not established, it is generally attributed to the presence of a cytoskeletal network (made of the proteins spectrin and ankyrin) that is anchored to the bilayer membrane of the RBCs.[19,41] Presumably, this network is able to withstand the processing steps employed here (osmotic stress and sonication) and remain intact in the NERs, giving them their characteristic shape. Thus, NERs appear to retain both the biochemical as well as morphological signatures of their parent RBCs, even though they are 1/10th the size of the RBCs. With respect to size, note that the hydrodynamic diameters of a disc and an equivalent sphere are expected to be nearly identical because D_h is dictated by the largest dimension of the object. This explains why similar D_h values were measured by DLS for the NERs in water and in buffer (Figure 2).

We also studied NERs using SANS. For this, we prepared a pellet of the micron-sized MERs as before and then suspended these in deuterium oxide (D_2O). This suspension was then sonicated to obtain the NERs. The use of D_2O ensures sufficient contrast between the scattering objects and the solvent under SANS. The scattered intensity I in SANS is measured as a function of the scattering vector q. For a dilute dispersion of weakly interacting vesicles, the intensity $I(q)$ can be accounted for purely in terms of the form factor $P(q)$ of the scatterers (i.e., the structure factor $S(q) \rightarrow 1$).[42] In turn, $I(q)$ is given by the following expression for the case where the vesicle radius R is large relative to the thickness t of the bilayer membrane:[42,43]

$$I(q) \sim (4\pi R)^2 \cdot \frac{t^2}{q^2} \sin^2(qR) \quad (1)$$

Equation 1 indicates that $I(q)$ for such vesicles should show a q^{-2} decay in the low q range. SANS data are plotted in Figure 4

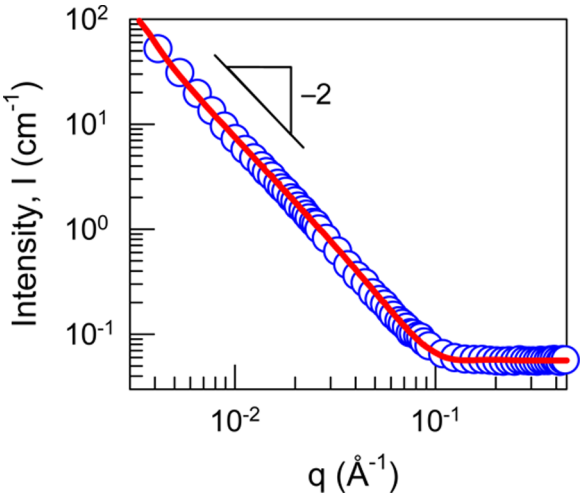

Figure 4. SANS spectra for NERs in D_2O. The intensity I follows a slope of −2 at low values of the scattering vector q. This is characteristic of unilamellar vesicles. The line through the data is a fit using a model for vesicles (eq 1).

for NERs at a number density of 1.6×10^{12} NERs/mL in D_2O. As expected, we find that the intensity I follows a slope of −2 at low and moderate q, which is indeed characteristic of unilamellar vesicles. (If the vesicles were multilamellar, we would see additional peak(s) at moderate q, corresponding to the interlamellar spacing.[42]) The above SANS data is not sensitive to the overall size of the vesicles because it falls outside the window of size scales probed by neutrons. However, it permits accurate estimation of the bilayer membrane thickness t. This value can be determined by replotting the above data in a cross-sectional Guinier plot, i.e., a plot of $\ln(Iq^2)$ versus q^2, which yields a straight line with a slope = $t^2/12$ (this is equivalent to fitting eq 1 to the data).[43] From this plot, we estimate $t \approx 4.5$ nm for these NERs. For comparison, previous measurements on human RBCs have reported the membrane thickness to be between 5 to 7 nm.[44−46]

Stability of NERs Compared to Liposomes. Our studies using SANS and cryo-TEM reveal that the structure of NERs is quite comparable to that of liposomes (both are unilamellar vesicles). Figure 2 also showed that the NERs are stable structures, i.e., they exhibit approximately the same size over several days. We now compare in more detail the stability of NERs against that of liposomes. First, we prepared conventional liposomes using the phospholipid DPPC and cholesterol in a 60:40 molar ratio. DPPC has two palmitoyl (C_{16}, saturated) tails and a zwitterionic phosphocholine headgroup. Since DPPC is zwitterionic and cholesterol is uncharged, DPPC/cholesterol liposomes have a negligible surface charge. Next, we prepared liposomes with PEG surface moieties by combining DPPC, cholesterol, and a third lipid, DOPE-mPEG in a molar ratio of 55:40:5. The latter has two oleyl (C_{18}, unsaturated) tails and an anionic phosphoethanolamine headgroup attached to a PEG moiety of molecular weight 2000 Da. The anionic headgroups of DOPE-mPEG impart a net negative charge to the liposomes. We chose these two

DOI: 10.1021/acs.langmuir.5b03014
Langmuir 2016, 32, 171−179

liposomal compositions based on our previous experience with them.[47] Both had been found to be relatively stable when prepared in PBS buffer and stored in a refrigerator.

To compare the liposomes and the NERs under more aggressive conditions, we studied each sample in the presence of serum, which is the solution component of blood that is rich in proteins and salts. Serum contains a variety of proteins, especially those that are a part of the immune system such as antibodies.[19] The stability of nanostructures in serum is particularly important for drug-delivery applications, and, as noted earlier, liposomes often show poor stability in serum.[16,17] Figure 5a shows the normalized sizes of the three structures in serum over time. At time $t = 0$, all three had mean diameters around 100 nm, and this was also their diameter in aqueous buffer. The zeta potentials of the three in serum were measured to be 0.4 mV, − 48 mV, and −38 mV, for the bare liposomes, PEGylated liposomes, and the NERs, respectively. Figure 5a shows that the bare liposomes are relatively unstable, with their size increasing by a factor of about 2.5 over the first 24 h in serum (this is indicative of aggregation into larger structures).

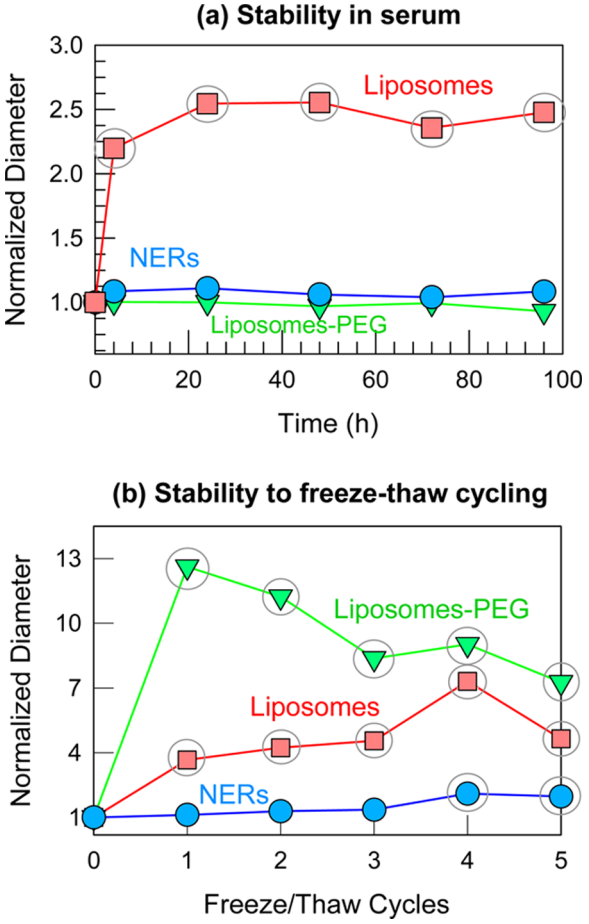

Figure 5. Stability of NERs compared to bare liposomes and PEGylated liposomes. (a) Size (normalized to its value at $t = 0$) over time in serum. The NERs and the PEGylated liposomes maintain their size, while the bare liposomes show significant aggregation (increase in size). The circles around the points indicate that a precipitate was observed at the bottom of the sample vial. (b) Size (normalized to its initial value) after freeze−thaw cycling. The NERs maintain their size (some precipitation is seen after four cycles), while the other samples show an increase in size and significant precipitation after just one cycle.

Moreover, the liposome samples exhibited a precipitate at the bottom of the vial within 4 h of preparation. The sample also turned from bluish to colorless as a result of the precipitation; this indicates that a large fraction of the liposomes were in the precipitate. In comparison, both the PEGylated liposomes and the NERs remained stable (no change in size and no precipitation) over a period of 96 h. The higher stability of the latter two correlates with their more negative surface charge as well as the presence of steric-stabilizing moieties attached to the membrane. As mentioned, the stabilizing moieties in the case of the NERs are expected to be hydrophilic sugars attached to membrane proteins or lipids.

Another issue is the stability of liposomes to freeze−thaw cycling.[18] During freezing, ice crystals can form inside a liposome, and the expansion of ice can rupture the membrane. When the sample is thawed, ideally the liposome should revert to its original size and structure. We subjected the three above samples to a number of freeze−thaw cycles and measured their size at the end of each cycle. The results in Figure 5b reveal that the NERs are much more stable to freeze−thaw cycling than the bare or PEGylated liposomes. In the latter two cases, a solid precipitate was found in each sample after just one freeze−thaw cycle and the precipitation worsened with each such cycle (the sample above the precipitate still remained a bluish solution). In the case of the NERs, only slight precipitation was found and that too only after 4 cycles. Also, the size of the bare liposomes and PEGylated liposomes left in solution significantly increased upon freeze−thaw cycling, indicating aggregation, whereas the size of the NERs remained relatively constant even after five such cycles. We speculate that the continued presence of the spectrin-ankyrin filamentous network attached to the NER membrane[19] (this was postulated in the previous section to explain the biconcave shape in Figure 3b) is responsible for the greater stability of the NERs.

Solute Encapsulation in NERs and Subsequent Release. Liposomes are used in drug delivery because of their ability to encapsulate solutes in their aqueous interior and release them slowly into the external environment. We now examine whether similar solute encapsulation and release can be done with NERs. As a solute, we chose dextran-FITC, i.e., the polysaccharide dextran (molecular weight ∼4 kDa) attached to the fluorescent dye, fluorescein isothiocyanate (FITC). To encapsulate the solute in the NERs, we first added the solute to the MER suspension at room temperature and then sonicated the sample. The shear from sonication partially ruptures the MER membranes as they rearrange into NERs; during this process, some of the solute is internalized. We then subjected the sample to a "resealing" procedure involving a freeze-anneal-thaw cycle (cool to 4 °C, then warm and anneal at 37 °C, then cool back to room temperature). This resealing procedure has been widely used by other researchers over the years with MERs.[23,24] At the end of this process, the NERs are expected to have intact, sealed membranes. At this point, while the NERs are loaded with solute, free solute is also present in the external solution. To remove the free solute, the sample is purified through a size exclusion column. The resulting NERs have the solute only inside them. This sample is then placed in a dialysis cassette (Figure 6a), which in turn is placed in an external buffer solution (the buffer is in large excess compared to the sample volume). This point corresponds to $t = 0$ for the release experiments. We chose a dialysis membrane with a 12 kDa cutoff, which is sufficiently large to allow the dextran-FITC solute to pass through it. Release of solute from the NERs to

DOI: 10.1021/acs.langmuir.5b03014
Langmuir 2016, 32, 171−179

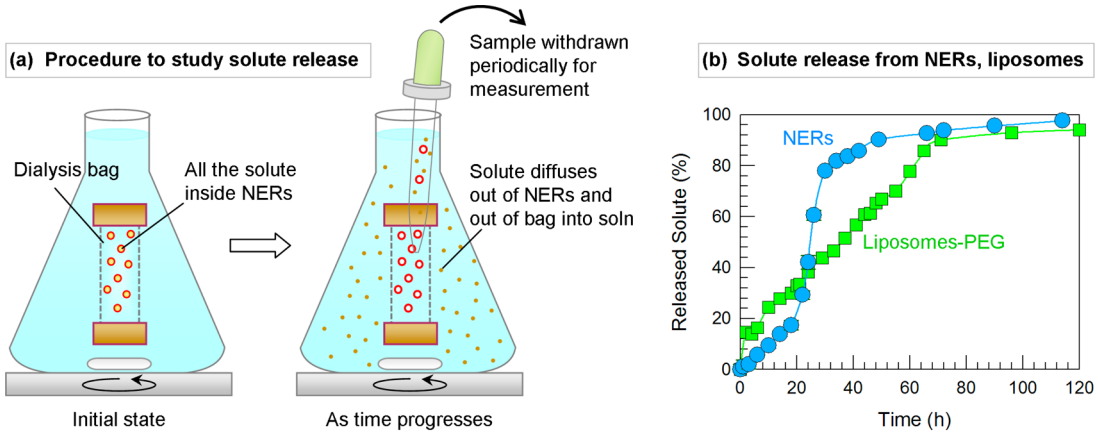

Figure 6. Comparison of solute release from NERs and liposomes. A schematic of the procedure is shown in (a). The sample of interest is in a dialysis bag, which is placed in excess buffer. The solute is dextran-FITC, which is loaded into either NERs or liposomes. As the solute diffuses out of these structures and into the buffer, the concentration in the dialysis bag keeps decreasing. This concentration is monitored over time, and the data are used to construct the release curves shown in (b).

the external buffer was then monitored over time by periodically measuring the fluorescence of the solution in the dialysis cassette (Figure 6a). For comparison with the NERs, a similar experiment was also done with the PEGylated liposomes (i.e., DPPC/cholesterol/DOPE-mPEG) that were discussed earlier in Figure 5.

Figure 6b shows release curves for dextran-FITC from the NERs and the liposomes. In the case of the liposomes, the release occurs at a nearly constant rate over the first 72 h, and thereafter it slows down. In the case of the NERs, the release is slower over the first 20 h, but then it picks up over the next 20 h, and finally, once about 80% of the solute is released, the rate of release slows down again. The NERs release <10% of the solute over the first 10 h compared to the liposomes (~25% over the first 10 h). On the other hand, 90% of the solute is released by the NERs within 50 h compared to 75 h in the case of the liposomes. Note that a clean comparison between NERs and liposomes is not easy to make. While the NER sample contained about 1.6×10^{12} NERs/mL, the liposome sample had about 1×10^{13} liposomes/mL (both the NERs and liposomes had similar sizes, i.e., ~ 100 nm). Also, the same concentration of solute was introduced into both samples at the outset, but the encapsulation efficiencies of the two structures were quite different. The total loading of dextran-FITC (from the readings as $t = 0$) was 40 μg/mL in the NERs and 20 μg/mL in the liposomes. Thus, the NERs were able to encapsulate more of the solute even though there were fewer of them. Additional studies are needed to further clarify these aspects. But from these initial studies, we can already see that the NERs, much like the liposomes, can be applied toward the controlled release of solutes.

Targeting Antibody-Conjugated NERs to Specific Cell Types. Many biomedical applications involve the use of immunoliposomes, which have targeting agents such as antibodies conjugated to their external surface.[7,9] Such structures can target and bind specifically to cells with receptors for the targeting agents (binding is usually followed by internalization into the cells through endocytosis). We wanted to examine whether such targeting could be carried out with surface-modified NERs. For this, we began with protein G, which is a protein derived from *Streptococcal* bacteria that has the ability to bind to the constant (Fc) region of antibodies.[48,49] We used an enzyme called microbial trans-glutaminase (mTG) to conjugate protein G to the NER membrane (Figure 7a).[49,50] The protein G was engineered with a glutamine (Gln) tag for this purpose.[50] mTG creates covalent bonds between the glutamine on protein G and lysine residues on NER membrane proteins.[49] The mTG reaction is sufficiently mild so that the

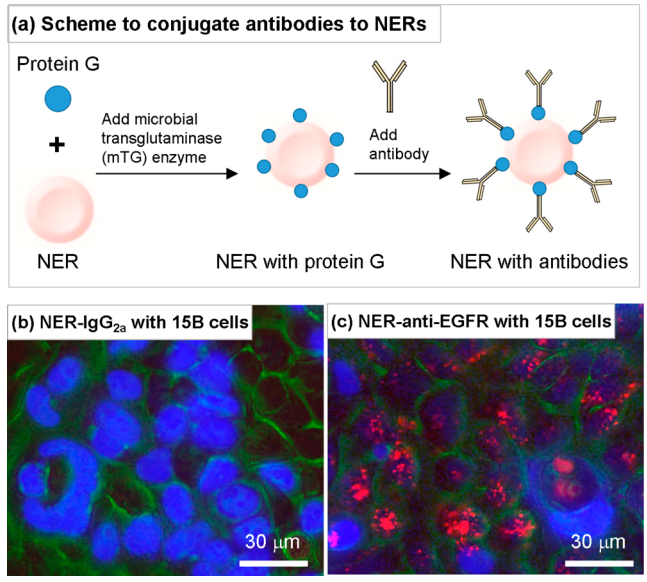

Figure 7. NERs with antibodies are demonstrated to target cells with the right receptors. In (a), the scheme to conjugate antibodies to the NER membranes is shown. This has two steps: first, protein G is covalently attached to NER membranes using the enzyme microbial transglutaminase (mTG). Then self-assembly is induced between protein G and the Fc region of added antibodies, resulting in the creation of NERs with anchored antibodies. In (b) and (c), NERs with different antibodies are tested against 15B cells, which are a class of tumor cells known to overexpress EGFR in their membranes. The NERs are tagged with a red-fluorescent lipid. In the control case, when the antibody is a nonspecific IgG_{2a}, no binding to the cells is seen in the fluorescence image in (b). Conversely, when the antibody is an anti-EGFR, the NERs show considerable binding to the 15B cells, as seen from the red fluorescence in the image in (c). The blue color in (b) and (c) is from DAPI counterstain of the nuclei in the cells. The green color is the cell boundary, evident from the bright-field image and superposed on the fluorescence images.

DOI: 10.1021/acs.langmuir.5b03014
Langmuir 2016, 32, 171−179

conjugated proteins retain their activity. To these NERs modified with protein G, we then added an anti-EGFR antibody, where EGFR refers to the epidermal growth factor receptor (this receptor is frequently overexpressed on many kinds of tumor cells[47,51]). Self-assembly then occurs between protein G and the Fc region of the antibodies, allowing the antibodies to be anchored in the right orientation for recongnizing antigens via their Fab regions (Figure 7a).[49] The final result of this process is to generate NERs functionalized with anti-EGFR antibodies. Note that the NER membranes are also tagged with a red-fluorescent lipid called DiI to aid in visualization.

To test these NERs, we selected the 15B cell line, which is a class of squamous cell carcinoma of the head and neck (SCCHN). These tumor cells are known to overexpress EGFRs on their membranes.[47,51] The cells and the NERs with anti-EGFR were incubated for 30 min, followed by washing to remove unbound structures. As a control, we also synthesized NERs with a different antibody (mouse IgG_{2a}) that has no affinity for EGFR. Figure 7 shows images from fluorescence microscopy for the two cases. The NERs with anti-EGFR show substantial binding to the 15B cells as seen by the significant red fluorescence (Figure 7c). In the control case, there is negligible binding of the NERs to the 15B cells, as noted from the absence of red fluorescence (Figure 7b). Thus, we have preliminary evidence for specific binding of NERs to target cells with the right receptors. Further experiments are needed to confirm this binding specificity. Nevertheless, our preliminary results do indicate that NERs functionalized with antibodies can serve as targeting agents, i.e., that NERs can have many of the same functions and capabilities as liposomes.

CONCLUSIONS

In this study, we extracted erythrocytes from bovine blood and converted these into nanoerythrosomes (NERs). This was done by using osmotic gradients to remove the hemoglobin, and then sonicating the empty structures. NERs are found to be nanodiscs/spheres with an average diameter ∼110 nm, enclosed by a unilamellar bilayer membrane of thickness ∼4.5 nm. Compared to liposomes, NERs show improved colloidal stability in serum, and are more stable to freeze−thaw cycling. Much like liposomes, NERs can encapsulate solutes (including macromolecules) in their aqueous core, and these can be subsequently released by diffusion through the bilayer. NERs can also be decorated with targeting agents like antibodies, and such NERs can bind specifically to cells that have the receptors for the antibodies. In other words, NERs have many of the same capabilities as conventional liposomes, but with the added advantage of better colloidal stability. This improved stability is evidently because much of the membrane proteins and glycolipids attached to the blood cell membrane are still intact in the case of the NERs. While the presence of these membrane-bound molecules is beneficial in this context, there is also the risk of an immune response to these molecules if NERs were injected into a foreign species. However, there is the possibility of harvesting NERs from a patient's own blood. This possibility can become more realistic if NER preparation and functionalization can be performed at the bedside, possibly using lab-on-a-chip devices. Such NERs may potentially offer several benefits including biocompatibility, minimization of immune response, and possibly also an extended circulation time[52] in the body.

MATERIALS AND METHODS

Materials. Bovine blood was purchased from Lampire. The lipids 1,2-dipalmitoyl-*sn*-glycero-3-phosphocholine (DPPC); 1,2-dioleoyl-*sn*-glycero-3-phospho-ethanolamine-*N*-(biotinyl) (sodium salt) (DOPE-Biotin); and 1,2-dioleoyl-*sn*-glycero-3-phosphoethanolamine-*N*-[methoxy-(polyethylene glycol)-2000] (DOPE-mPEG) were purchased from Avanti Polar Lipids. Cholesterol and dextran-FITC were from Sigma-Aldrich. The fluorescent lipid 1,1′-diocta-decyl-3,3,3′,3′-tetramethyl-indo-carbocyanine perchlorate (DiI) was from Molecular Probes. Phosphate buffered saline (PBS) and fetal bovine serum (FBS) were from Life Technologies. The dialysis cassette was from Thermo Fisher Scientific. The antibodies, mouse anti-EGFR (sc-120) and a control mouse IgG_{2a} (sc-3878) were purchased from Santa Cruz Biotechnology. The microbial trans-glutaminase (mTG) enzyme and the protein G with a glutamine tag were provided by the Bentley lab at UMD.[50]

NER Preparation. The procedure for preparing NERs was described schematically in Figure 1. This procedure is adapted from that used in previous studies[24,33] with some modifications. First,100 mL of bovine whole blood was taken, and RBCs were separated from it by centrifuging three times (2000 rpm, 10 min). Between each step, the RBCs at the bottom of the tube were washed and resuspended in PBS. After the third step, the RBCs were transferred to a hypotonic solution to remove the hemoglobin. The hypotonic solution was composed of PBS with 0.14 M NaCl, 10 mM Na-phosphate, and 3 mM KCl. The RBCs were incubated in the hypotonic PBS for 5 min on ice. This was then transferred to an ultracentrifuge (Beckman SW28) and run at 12 000 rpm for 10 min at 4 °C. The pellet (cells with hemoglobin removed) was collected and resuspended in the hypotonic PBS, and this process was repeated thrice. Subsequently, the sediment was resuspended in cold PBS and ultracentrifuged at 20 000 rpm for 10 min at 4 °C; this was again repeated thrice. The final pellet contains the washed MERs (Figure 1e). These MERs were placed in PBS (pH of 7.4), and this solution was ultrasonicated using a probe sonicator (Qsonica) at 47.5 W for 15 min to give the NERs.

Liposome Preparation. Two types of liposomes were prepared according to previous procedures.[47] Bare liposomes contained a mixture of DPPC:Cholesterol = 60:40 (molar ratio). PEGylated liposomes employed a mixture of DPPC:Cholesterol:DOPE-mPEG = 55:40:5 (molar ratio). The pertinent lipid mixture was dissolved in chloroform, and a dried film was formed by evaporating the solvent with a dry nitrogen stream, followed by vacuum desiccation for 24 h. The lipid film was rehydrated with PBS and stirred at 60 °C for 2 h. The mixture was then ultrasonicated at 47.5 W for 15 min using a probe sonicator (Qsonica) to give liposomes. Samples were maintained at 4 °C before experiments. The total lipid concentration in both the final samples was 6 mM.

Cell and Particle Count. The number densities of RBCs and MERs (microscale structures) were determined using a hemocytometer (Fisher Scientific). Trypan blue was used to provide contrast to the structures before the counts were taken.

Size Measurement. Sizes of nanostructures were measured by dynamic light scattering (DLS) at 25 °C using a Photocor-FC instrument. The instrument has a 5 mW laser light source at 633 nm, and the scattering angle was fixed at 90°. All measurements were done in triplicate, and the average values are shown.

Zeta Potential Measurements. Zeta potentials of the various nanostructures were measured by a Laser Doppler Velocimetry technique using a Malvern Zetasizer NanoZS90 at a 90° scattering angle. Samples were placed in disposable polystyrene cuvettes. All measurements were done in triplicate, and the average values are reported..

Cryo-Transmission Electron Microscopy (Cryo-TEM). C-Flat holey carbon grids with a hole size of 1.2 μm were purchased from Electron Microscopy Sciences. Grids bearing aqueous solutions of the nanostructures were plunged into liquid ethane (−183 °C) using a Gatan CryoPlunge3, so as to form vitrified specimens. The samples were thereafter imaged on a JEOL-2100 LaB6 TEM at liquid nitrogen temperature.

DOI: 10.1021/acs.langmuir.5b03014
Langmuir 2016, 32, 171−179

Small-Angle Neutron Scattering (SANS). Measurements were made on the NG-7 (30 m) beamline at NIST in Gaithersburg, MD. Neutrons with a wavelength of 6 Å were selected. Three sample−detector distances were used to probe a range of scattering vectors from 0.004 to 0.4 $Å^{-1}$. Samples were studied in 2 mm quartz cells at 25 °C. The scattering spectra were corrected and placed on an absolute scale using calibration standards provided by NIST. The data are shown for the radially averaged intensity I as a function of the scattering vector $q = (4\pi/\lambda)\sin(\theta/2)$, where λ is the neutron wavelength and θ is the scattering angle.

Stability Tests. To assess colloidal stability, the two liposome samples and the NERs were first studied in the presence of FBS. This involved adding 1 mL of FBS to 2 mL of the above samples. Sizes were measured periodically by DLS. Next, the same samples were subjected to freeze−thaw cycling. During each cycle, the samples were frozen at −20 °C for 24 h and then thawed at room temperature for 2 h. Size changes were measured by DLS after every cycle. All measurements were conducted in triplicate (three samples from the same preparation), and the average values are plotted.

Solute Encapsulation. To encapsulate the solute (dextran-FITC) in the NERs, the following procedure was used. The starting point was with the pellet of MERs, which was obtained as described above. This pellet was combined with 1 mg/mL of the solute in PBS, followed by sonication as above. This converts the MERs to NERs and the solute is internalized during this process. The next step was to "reseal" the disrupted NER membranes to ensure that the solute remains inside. For this, the sample was subjected to a freeze-anneal-thaw cycle. That is, the sample was cooled to 4 °C, then immediately transferred to a water bath at 37 °C and annealed at that temperature for 40 min, then cooled back to room temperature. At the end of this cycle, we have "sealed" NERs containing the solute, but there is also free solute in the outer solution. To remove free solute, the solution was purified using size-exclusion chromatography (SEC), i.e., by passing it through a 1 × 20 cm column packed with Sephadex G50 resin (from Sigma-Aldrich). The same dextran-FITC solute was also encapsulated in the PEGylated liposomes. In this case, 1 mg/mL of the solute was added to the solution used to rehydrate the lipid film. The mixture was sonicated as before and then purified by SEC using the same column as above.

Solute Release Studies. Release of the dextran-FITC solute from the liposomes and the NERs was measured as follows. First, 3 mL of the pertinent sample was injected into the dialysis cassette, which was then placed into a large flask containing 1 L of PBS buffer (see Figure 6a). The buffer was replaced with fresh buffer every 1 h at the outset and thereafter every 4 h. 120 μL of sample was collected periodically from the dialysis bag and the fluorescence intensity of solute in the sample was measured by a SpectraMax M2 spectrometer (Molecular Devices) (Ex: 492 nm, Em: 518 nm). These were converted to concentrations using a standard curve. As the solute is released into the external buffer, the solute concentration in the bag keeps decreasing. These data were normalized into release curves, as shown in Figure 6b.

Antibody Conjugation. To conjugate the antibody to NERs, the following procedure was used, as shown schematically in Figure 7a. For this, stock solutions of Gln-tagged protein G (50 μg/mL) and mTG enzyme (20 units/mL) were obtained from the Bentley lab. First, protein G was covalently linked to the NERs using mTG (Figure 7a). To accomplish this, the NERs were combined with protein G (2.5 μg/mL) and mTG (0.08 units/mL), and the mixture was subjected to mild shaking at room temperature for 30 min. Then the NERs with protein G were washed and purified using a centrifugal filter tube with a 100 kDa cutoff (this removes any unreacted protein G). The structures were resuspended in PBS and then 10^{14} antibody molecules were added. This mixture was incubated overnight at 4 °C under mild shaking. Antibody-laden NERs were then purified by centrifugation as above. For visualization by fluorescence microscopy, the same NERs were also tagged with a fluorescent lipid dye called DiI. This was done during the NER formation process: 2 μM DiI was dissolved in ethanol, and 20 μL of this solution was added to 1 mL of the MERs, followed by sonication to yield NERs.

Cell Lines. SCCHN 15B cells were provided by Dr. Jennifer Grandis (University of Pittsburgh). Cells were cultured in RPMI-1640 medium with 10% FBS and 1% L-glutamine (from Sigma-Aldrich). Cells were maintained at 37 °C in 5% CO_2.

Cell Targeting Studies. 10^4 15B cells were seeded onto an 8 well chamber slide at 37 °C. Cells were propagated to 80% confluency (typically overnight). RPMI medium containing 1% bovine serum albumin (BSA) was then added to the cells for 30 min. The BSA eliminates nonspecific binding of the antibodies to the cells. Two DiI-tagged NER samples were studied, one with the NERs bearing the mouse IgG_{2a} (control) antibody and the other with the NERs bearing the anti-EGFR antibody. 100 μL of each sample was added to separate wells containing the 15B cells and left to incubate for 30 min. Thereafter, the cells were washed three times with PBS to remove unbound nanostructures. The samples were then fixed with 2% paraformaldehyde. Cells were then stained with 4′,6′-diamidino-2-phenylindole (DAPI) (EMD Chemicals), which is a dye that binds to the nuclei in the cells. Then the cells were visualized under a fluorescence microscope.

AUTHOR INFORMATION

Corresponding Authors

*E-mail: sraghava@umd.edu

*E-mail: wdsou001@umaryland.edu

Notes

The authors declare no competing financial interest.

ACKNOWLEDGMENTS

We acknowledge Dr. Wen-An Chiou from the NISP lab at UMD for assistance with the cyro-TEM studies. We thank NIST for facilitating the SANS experiments performed as part of this work, and we are grateful to Dr. Hyuntaek Oh for his help with conducting these experiments and with analyzing SANS data. Finally, we wish to thank Dr. Chen-Yu Tsao, Dr. Yi Liu, and Prof. Greg Payne for providing access to resources in their lab for biomolecular characterization.

REFERENCES

(1) Lasic, D. D. *Liposomes: From Physics to Applications*; Elsevier: Amsterdam, 1993.

(2) Bangham, A. D.; Horne, R. W. Negative staining of phospholipids and their structural modification by surface-active agents as observed in the electron microscope. *J. Mol. Biol.* **1964**, *8*, 660−8.

(3) Sessa, G.; Weissman, G. Phospholipid spherules (liposomes) as a model for biological membranes. *J. Lipid Res.* **1968**, *9*, 310−318.

(4) Szoka, F.; Papahadjopoulos, D. Comparative properties and methods of preparation of lipid vesicles (liposomes). *Annu. Rev. Biophys. Bioeng.* **1980**, *9*, 467−508.

(5) Lasic, D. D. The mechanism of vesicle formation. *Biochem. J.* **1988**, *256*, 1−11.

(6) Gregoriadis, G. Engineering liposomes for drug delivery: Progress and problems. *Trends Biotechnol.* **1995**, *13*, 527−537.

(7) Torchilin, V. P. Recent advances with liposomes as pharmaceutical carriers. *Nat. Rev. Drug Discovery* **2005**, *4*, 145−160.

(8) Jesorka, A.; Orwar, O. Liposomes: Technologies and analytical applications. *Annu. Rev. Anal. Chem.* **2008**, *1*, 801−832.

(9) Rongen, H. A. H.; Bult, A.; vanBennekom, W. P. Liposomes and immunoassays. *J. Immunol. Methods* **1997**, *204*, 105−133.

(10) Nobs, L.; Buchegger, F.; Gurny, R.; Allemann, E. Current methods for attaching targeting ligands to liposomes and nanoparticles. *J. Pharm. Sci.* **2004**, *93*, 1980−1992.

(11) Armengol, X.; Estelrich, J. Physical stability of different liposome compositions obtained by extrusion method. *J. Microencapsulation* **1995**, *12*, 525−535.

(12) Woodle, M. C.; Lasic, D. D. Sterically stabilized liposomes. *Biochim. Biophys. Acta, Rev. Biomembr.* **1992**, *1113*, 171−199.

DOI: 10.1021/acs.langmuir.5b03014
Langmuir 2016, 32, 171−179

(13) Allen, T. M. Long-circulating (sterically stabilized) liposomes for targeted drug-delivery. *Trends Pharmacol. Sci.* **1994**, *15*, 215−220.
(14) Moghimi, S. M.; Szebeni, J. Stealth liposomes and long circulating nanoparticles: critical issues in pharmacokinetics, opsonization and protein-binding properties. *Prog. Lipid Res.* **2003**, *42*, 463−478.
(15) Zhang, L. F.; Granick, S. How to stabilize phospholipid liposomes (using nanoparticles). *Nano Lett.* **2006**, *6*, 694−698.
(16) Jones, M. N.; Nicholas, A. R. The effect of blood-serum on the size and stability of phospholipid liposomes. *Biochim. Biophys. Acta, Biomembr.* **1991**, *1065*, 145−152.
(17) Wytrwal, M.; Bednar, J.; Nowakowska, M.; Wydro, P.; Kepczynski, M. Interactions of serum with polyelectrolyte-stabilized liposomes: Cryo-TEM studies. *Colloids Surf., B* **2014**, *120*, 152−159.
(18) Costa, A. P.; Xu, X. M.; Burgess, D. J. Freeze-anneal-thaw cycling of unilamellar liposomes: Effect on encapsulation efficiency. *Pharm. Res.* **2014**, *31*, 97−103.
(19) Alberts, B. *Molecular Biology of the Cell*; Garland Publishers: New Yok, 2002.
(20) Hoffman, J. F. Physiological characteristics of human red blood cell ghosts. *J. Gen. Physiol.* **1958**, *42*, 9−28.
(21) Ihler, G. M.; Glew, R. H.; Schnure, F. W. Enzyme loading of erythrocytes. *Proc. Natl. Acad. Sci. U. S. A.* **1973**, *70*, 2663−2666.
(22) Cuppoletti, J.; Mayhew, E.; Zobel, C. R.; Jung, C. Y. Erythrosomes: Large proteoliposomes derived from crosslinked human erythrocyte cytoskeletons and exogenous lipid. *Proc. Natl. Acad. Sci. U. S. A.* **1981**, *78*, 2786−90.
(23) Lewis, D. A.; Alpar, H. O. Therapeutic possibilities of drugs encapsulated in erythrocytes. *Int. J. Pharm.* **1984**, *22*, 137−146.
(24) Hirlekar, R. S.; Patel, P. D.; Dand, N.; Kadam, V. J. Drug loaded erythrocytes: A novel drug delivery system. *Curr. Pharm. Des.* **2008**, *14*, 63−70.
(25) Al-Achi, A.; Boroujerdi, M. Pharmacokinetics and tissue uptake of doxorubicin associated with erythrocyte-membrane - Erythrocyte-ghosts vs erythrocyte-vesicles. *Drug Dev. Ind. Pharm.* **1990**, *16*, 2199−2219.
(26) Lejeune, A.; Moorjani, M.; Gicquaud, C.; Lacroix, J.; Poyet, P.; Gaudreault, R. Nanoerythrosome, a new derivative of erythrocyte ghost: preparation and antineoplastic potential as drug carrier for daunorubicin. *Anticancer Res.* **1994**, *14*, 915−9.
(27) Moorjani, M.; Lejeune, A.; Gicquaud, C.; Lacroix, J.; Poyet, P.; Gaudreault, R. C. Nanoerythrosomes, a new derivative of erythrocyte ghost 0.2. Identification of the mechanism of action. *Anticancer Res.* **1996**, *16*, 2831−2836.
(28) Lejeune, A.; Poyet, P.; Gaudreault, R. C.; Gicquaud, C. Nanoerythrosomes, a new derivative of erythrocyte ghost 0.3. Is phagocytosis involved in the mechanism of action? *Anticancer Res.* **1997**, *17*, 3599−3603.
(29) Desilets, J.; Lejeune, A.; Mercer, J.; Gicquaud, C. Nanoerythrosomes, a new derivative of erythrocyte ghost: IV. Fate of reinjected nanoerythrosomes. *Anticancer Res.* **2001**, *21*, 1741−1747.
(30) Pouliot, R.; Saint-Laurent, A.; Chypre, C.; Audet, R.; Vitte-Mony, I.; Gaudreault, R. C.; Auger, M. Spectroscopic characterization of nanoErythrosomes in the absence and presence of conjugated polyethyleneglycols: an FTIR and (31)P-NMR study. *Biochim. Biophys. Acta, Biomembr.* **2002**, *1564*, 317−24.
(31) Agnihotri, J.; Gajbhiye, V.; Jain, N. K. Engineered cellular carrier nanoerythrosomes as potential targeting vectors for anti-malarial drug. *Asian J. Pharm.* **2010**, *4*, 116−120.
(32) Agnihotri, J.; Jain, N. K. Biodegradable long circulating cellular carrier for antimalarial drug pyrimethamine. *Artif. Cells, Nanomed., Biotechnol.* **2013**, *41*, 309−314.
(33) Gupta, N.; Patel, B.; Ahsan, F. Nano-engineered erythrocyte ghosts as inhalational carriers for delivery of fasudil: Preparation and characterization. *Pharm. Res.* **2014**, *31*, 1553−1565.
(34) Pal, G. K.; Pal, P. *Textbook of Practical Physiology*; Orient Longman: Calcutta [Great Britain], 2001.
(35) Hiemenz, P. C.; Rajagopalan, R. *Principles of Colloid and Surface Chemistry*, 3rd ed.; Marcel Dekker: New York, 1997.
(36) Hassan, P. A.; Rana, S.; Verma, G. Making sense of Brownian motion: Colloid characterization by dynamic light scattering. *Langmuir* **2015**, *31*, 3−12.
(37) Nelson, D. L.; Cox, M. M. *Lehninger Principles of Biochemistry*; W. H. Freeman: New York, 2008.
(38) Danino, D.; Bernheim-Groswasser, A.; Talmon, Y. Digital cryogenic transmission electron microscopy: an advanced tool for direct imaging of complex fluids. *Colloids Surf., A* **2001**, *183*, 113−122.
(39) Almgren, M.; Edwards, K.; Karlsson, G. Cryo transmission electron microscopy of liposomes and related structures. *Colloids Surf., A* **2000**, *174*, 3−21.
(40) Danino, D. Cryo-TEM of soft molecular assemblies. *Curr. Opin. Colloid Interface Sci.* **2012**, *17*, 316−329.
(41) Diez-Silva, M.; Dao, M.; Han, J. Y.; Lim, C. T.; Suresh, S. Shape and biomechanical characteristics of human red blood cells in health and disease. *MRS Bull.* **2010**, *35*, 382−388.
(42) Pedersen, J. S. Analysis of small-angle scattering data from colloids and polymer solutions: modeling and least-squares fitting. *Adv. Colloid Interface Sci.* **1997**, *70*, 171−210.
(43) Kucerka, N.; Kiselev, M. A.; Balgavy, P. Determination of bilayer thickness and lipid surface area in unilamellar dimyristoyl phosphatidylcholine vesicles from small-angle neutron scattering curves: A comparison of evaluation methods. *Eur. Biophys. J.* **2004**, *33*, 328−334.
(44) McCaughan, L.; Krimm, S. X-ray and neutron scattering density profiles of the intact human red blood cell membrane. *Science* **1980**, *207*, 1481−3.
(45) Hochmuth, R. M.; Evans, E. A.; Wiles, H. C.; McCown, J. T. Mechanical measurement of red-cell membrane thickness. *Science* **1983**, *220*, 101−102.
(46) Scheffer, L.; Bitler, A.; Ben-Jacob, E.; Korenstein, R. Atomic force pulling: probing the local elasticity of the cell membrane. *Eur. Biophys. J.* **2001**, *30*, 83−90.
(47) Kuo, Y. C.; Hung, C. W.; Gullapalli, R. P.; Xu, S.; Zhuo, J. C.; Raghavan, S. R.; D'Souza, W. D. Liposomal nanoprobes that combine anti-EGFR antibodies and MRI contrast agents: Synthesis and in vitro characterization. *RSC Adv.* **2014**, *4*, 33756−33764.
(48) Wu, H. C.; Shi, X. W.; Tsao, C. Y.; Lewandowski, A. T.; Fernandes, R.; Hung, C. W.; DeShong, P.; Kobatake, E.; Valdes, J. J.; Payne, G. F.; Bentley, W. E. Biofabrication of antibodies and antigens via IgG-binding domain engineered with activatable pentatyrosine protag. *Biotechnol. Bioeng.* **2009**, *103*, 231−240.
(49) Payne, G. F.; Kim, E.; Cheng, Y.; Wu, H. C.; Ghodssi, R.; Rubloff, G. W.; Raghavan, S. R.; Culver, J. N.; Bentley, W. E. Accessing biology's toolbox for the mesoscale biofabrication of soft matter. *Soft Matter* **2013**, *9*, 6019−6032.
(50) Liu, Y.; Terrell, J. L.; Tsao, C. Y.; Wu, H. C.; Javvaji, V.; Kim, E.; Cheng, Y.; Wang, Y. F.; Ulijn, R. V.; Raghavan, S. R.; Rubloff, G. W.; Bentley, W. E.; Payne, G. F. Biofabricating multifunctional soft matter with enzymes and stimuli-responsive materials. *Adv. Funct. Mater.* **2012**, *22*, 3004−3012.
(51) Kalyankrishna, S.; Grandis, J. R. Epidermal growth factor receptor biology in head and neck cancer. *J. Clin. Oncol.* **2006**, *24*, 2666−72.
(52) Hu, C. M. J.; Zhang, L.; Aryal, S.; Cheung, C.; Fang, R. H.; Zhang, L. F. Erythrocyte membrane-camouflaged polymeric nanoparticles as a biomimetic delivery platform. *Proc. Natl. Acad. Sci. U. S. A.* **2011**, *108*, 10980−10985.

DOI: 10.1021/acs.langmuir.5b03014
Langmuir 2016, 32, 171−179